Desertification of Bengal Dryland Areas Possible under Projected Climate Conditions

Dr. KARTIC BERA[*,#], Dr. MICHELLE E. NEWCOMER[**] and Prof. PABITRA BANIK[#]

[*]*Assistant Professor, Dept. of Pure and Applied Science, Midnapore City College, Kuturiya,*

Paschim Medinipur, West Bengal, India,

[**]*Research Scientist, Climate & Ecosystem Sciences Division, Lawrence Berkeley National Laboratory,*

Earth & Environmental Sciences Area, Berkeley, California, United States of America.

[#]*Former Post Doctoral Fellow & Professor. Agricultural and Ecological Research Unit, Indian Statistical Institute,*

203, Barrackpore Trunk Road, Kolkata – 700 108, West Bengal, India

e mail : banikpabitra@gmail.com

सार – शुष्क भूमि दुनिया भर में जलवायु परिवर्तन और मानवीय गतिविधियों के लिए सबसे संवेदनशील क्षेत्रों में से एक है। भविष्य की जलवायु प्रवृत्ति परिदृश्यों का आकलन शुष्क भूमि प्रबंधन निर्णय लेने के लिए मूल्यवान व्यावहारिक जानकारी प्रदान करता है। हुआंग एट अल. (2017) के अनुसार, इस सदी तक वैश्विक शुष्क भूमि का 50% से अधिक विस्तार हो जाएगा, जिसमें अधिकतम (78%) नव विस्तारित शुष्क भूमि विकासशील देशों में होगी। शुष्क भूमि के विस्तार और मरुस्थलीकरण की संभावना को समझने, मरुस्थलीकरण को कम करने और रोकने के लिए प्रारंभिक कार्रवाई का मार्गदर्शन हेतु बंगाल शुष्क भूमि विस्तार के महत्वपूर्ण पूर्व सूचक चर (तापमान और वर्षा) की जांच करते हैं। तापमान और वर्षा (2022-2041) के लिए पूर्वाग्रह-सही CMIP6 अनुमानित जलवायु परिवर्तन डेटा के प्रवृत्ति विश्लेषण का उपयोग करते हुए, परिणाम संकेत देते हैं कि भविष्य में शुष्क भूमि का विस्तार तापमान में वृद्धि और मॉनसूनी वर्षा में गिरावट से संभव है। अगले दो दशकों (2022-2041) में बंगाल के शुष्क क्षेत्र +0.1 से +0.5 डिग्री सेल्सियस ऊष्ण होंगे और मॉनसून अवधि के दौरान कुल वर्षा -2.57 से -13.43 मिमी तक कम हो जाएगी। यह देखते हुए कि ये चर शुष्क भूमि विस्तार के महत्वपूर्ण पूर्व सूचक हैं क्योंकि वाष्पोत्सर्जन और मिट्टी की नमी में कमी को बढ़ाने में उनकी भूमिका है, अनुमान लगाया जा सकता है कि पानी की कमी, भूमि क्षरण और मरुस्थलीकरण से प्रभावित आबादी में वृद्धि एक संभावित परिणाम हो सकती है। यह शोध पत्र भविष्य की जलवायु परिस्थितियों में प्रभावी शुष्क भूमि प्रबंधन, जैव विविधता संरक्षण और भूमि उपयोग योजना के लिए महत्वपूर्ण जानकारी प्रदान करता है।

ABSTRACT. Drylands are some of the most sensitive areas to climate change and human activities around the globe. Assessment of future climate trend scenarios provides valuable practical information for dryland management decision-making. According to Huang *et al*. (2016), more than 50% of global drylands will expand by this century, with a maximum (78%) of newly expanded dryland occurring in developing countries. To understand the potential for expansion of drylands and desertification, we examine critical predictor variables (temperature and precipitation) of Bengal dryland expansion to guide early actions to mitigate and prevent desertification. Using trend analysis of bias-corrected CMIP6 projected climate change data for temperature and precipitation (2022-2041), results indicate that future dryland expansion is possible from increases in temperature and declines in monsoonal precipitation. Over the next two decades (2022-2041), Bengal dryland areas will be +0.1 to +0.5 °C warmer and rainfall will decrease by -2.57 to -13.43 mm total during the monsoon period. Given that these variables are critical predictors of dryland expansion due to their role in driving evapotranspiration and soil moisture deficits, we anticipate an increase in the population affected by water scarcity, land degradation and desertification may be a potential outcome. Our work provides information critical for effective dryland management, biodiversity conservation, and land-use planning under future climate conditions.

Key words – Climate change, Drylands, Desertification, Prediction, Decadal, Trend analysis.

1. Introduction

Drylands are regions where evaporation from surfaces and transpiration by plants (evapotranspiration) exceed precipitation (Huang *et al.*, 2016). According to the United Nations Environment Management Group, many drylands around the world are heavily impacted by climate change (UNEMG, 2011). Long-term climate patterns affect water availability, desertification potential, and the danger of increasing occurrence of droughts and floods (Jain & Kumar, 2012). The southwest (SW) monsoon is the only source of precipitation over dryland areas. Due to spatially heterogeneous rainfall distribution, and water demand exceeding water availability, large groundwater storage reservoirs are largely responsible for storage and transport of natural subsurface flow and for provisioning the region's water requirements (Jain & Kumar, 2012). Also, heavy rainfall in the monsoon months results in water scarcity in many parts of the region during the non-monsoon periods (Jain & Kumar, 2012) due to undulated topography creating flooding conditions that quickly result in lost water from basins. Therefore, dryland regions always suffer from insufficient water, both domestic (agriculture) and drinking. Understanding the water-energy balance of precipitation, evapotranspiration, streamflow and temperature through data collection (*e.g.* Sprenger *et al.*, 2022) and data analysis of future changes in these variables will be essential to prevent flooding, manage water resources such as through managed aquifer recharge (*e.g.* Uhlemann, *et al.*, 2022), save lives and property and secure economic activities. Insufficient rainfall has a substantial adverse influence on water supply, water quality (Arora *et al.*, 2020) and aquatic ecosystems (Rogers *et al.*, 2021; Matheus Carnevali *et al.*, 2021) which are additional secondary impacts to desertification. While many studies have attempted to determine trends in precipitation and temperature, most of these assess either annual or seasonal series of climate variables for some individual stations or groups of stations (Brahim *et al.*, (2017), Lal (2001), Sinha Ray *et al.* (2003), Kumar *et al.* (2010)). Past studies have indicated that there is no clear trend in average annual temperature and precipitation in and around the Bengal study area (Das *et al.* (2017), Jain and Kumar (2012)).

Accurate climate forecasting is challenging in operational water resources management because it requires downscaling and bias-correction of projected climatic grid cells to the local level (Lee *et al.*, 2018). Several methods are available for precipitation forecasting, such as numerical weather prediction (NWP) models, statistical methods and machine learning techniques (Hofmann *et al.*, 2008, Rasmussen *et al.*, 2006). Bias-corrected climate projection datasets exist that use Empirical Quantile Mapping (EQM) output from General Circulation Models (GCMs) of Coupled Model Intercomparison Project-6 (CMIP6) (*e.g.* Mishra *et al.* (2020 a, b)). Predictions of temperature and precipitation for different regions around the world vary considerably among 21 General Circulation Models (GCMs) used by the Intergovernmental Panel on Climate Change (IPCC) in its sixth assessment (Mortimore *et al.*, 2009). For example, it is highly likely that winter precipitation will increase in the tropics and Tibetan plateau, and there will be increased risk of drought in the Mediterranean and Central America (Mortimore *et al.*, 2009). These changes can have varied implications around the world from dryland expansion, greening of the Sahel (Herrmann *et al.*, 2005), greater risk of algal blooms (Cheng *et al.*, 2021) and vulnerability of fragile ecosystem structure along coastlines from water and sea-level variations (Enguehard *et al.*, 2022). Various studies on climate prediction and trend analysis have been published using GCMs on different spatial scales to help construct future climate scenarios (Lee *et al.*, 2018). While not all dryland regions are expected to become drier (IPCC 2007) in some (if not all) drylands, variability in crucial climate parameters (including the amount and distribution of temperature, precipitation and evapotranspiration) is expected to grow (UNEMG, 2011). Prior studies have investigated variable climatic trends for the Bengal dryland region and they have found a warming climate for the future (Sadhukhan *et al.*, 2003, Rath *et al.*, 2022). Our research builds upon these prior works and assesses future projection of climatic temperature and precipitation in the Bengal dryland region at the local scale which are the main factors responsible for potential desertification & dryland expansion in the next two decades (2022-2041).

2. Study area

The dryland study area of West Bengal extends geographically between 85° 40′ - 88° 15′ East longitude and 21° 45′ - 24° 45′ North latitude (Fig. 1), with an approximate areal size of 28,697 km^2 (25.47 % of the total area of West Bengal state). The area around the plateau and highlands is flanked by the eastern fringes of the Chota-Nagpur Plateau (Bera *et al.*, 2014) and mostly contains lateritic soils. Present temperature highs in summer average 45 °C and in winter average 10 °C. Average total annual rainfall is 1,250 mm driven by the Southwest monsoon which is the only source of precipitation in the area. With a total population of 17 million (Census of India, 2011) most people are involved in the agricultural sector, *i.e.*, agriculture, hunting, forestry and fisheries, so the projected climatic variability and change will have significant impacts on these populations.
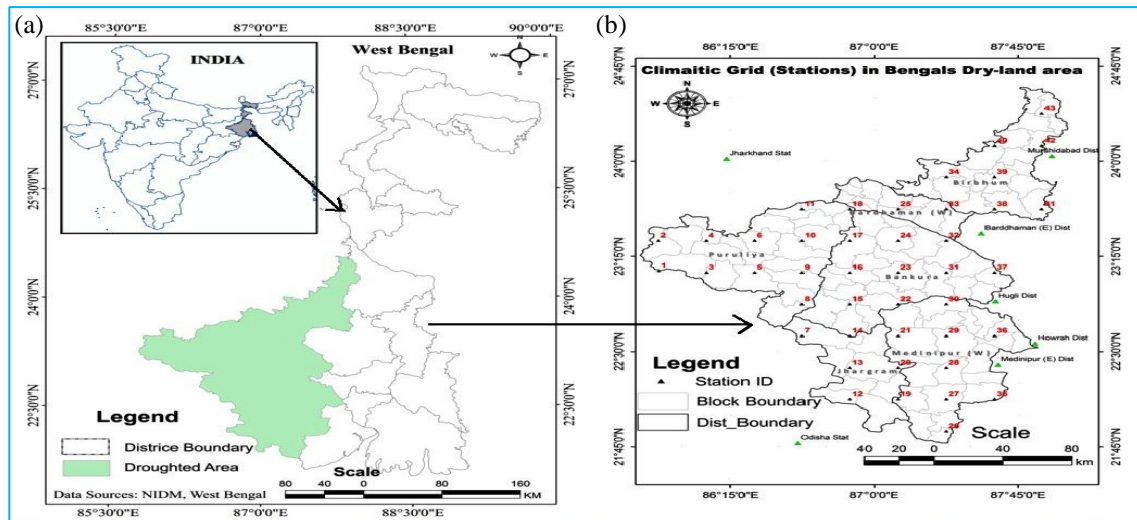
Figs. 1. (a &b). (a) Location map of the study area and the Bengal dryland region within India, (b) Map showing the grid locations that are associated with climate stations where on-the-ground observations are available. Grid cells #2, 7 and 26 will be referenced in later figs.

3.   Data & methods used

3.1. *Datasets used*

All datasets including bias-corrected, downscaled, and validated daily precipitation, minimum and maximum temperature CMIP6 data and historical data were provided by Mishra *et al.* (2020 a, b) for 13 GCM models and four shared socio-economic pathways (SSPs) including ssp126, ssp245, ssp370 and ssp585 for the period of 1951 to 2100. Historical gridded climate data (1951-2014) used in the validation procedure was provided by the India Meteorological Department (IMD) with 0.250 degree gridded spatial resolution and available from 1901-2018 (Mishra *et al.*, 2016, Pai *et al.*, 2014, Sheffield *et al.*, 2006). The period 1951-2014 represents the time period of the observed dataset that Mishra *et al.* (2020 a, b) used to develop the cumulative distribution functions (cdfs) and the transfer functions (described below). The raw historical and projected CMIP6-GCM climate data is available at a daily temporal resolution and 0.250 degree gridded spatial resolution from the CMIP6 project (https://esgf-node.llnl.gov/projects/cmip6/) however the bias-corrected, downscaled and validated data is already publically available (https://zenodo.org/records/3987736). For the purposes of this study, however, we used previously bias-corrected, downscaled, and validated datasets provided by Mishra *et al.* (2020 a, b) and we apply a novel application of this data for the Bengal study region, similar to the study design outlined by Singh *et al.* (2023). We discuss the brief details of the bias-correction procedure, downscaling, and validation below, however we refer the reader to Mishra *et al.* (2020 a, b) for additional details. The datasets that we have access to and used in this study do not include evapotranspiration (ET), unfortunately. While we acknowledge that historical and projected raw ET data might be available from the raw CMIP6 data sources, it is not a part of the published data provided to us by Mishra *et al.* (2020 a, b) which is already bias-corrected, downscaled, and validated. For the purposes of this study, we approximate the potential for desertification by analyzing both warming (temperature, °C) and drying (precipitation, mm) trends.

3.2. *Bias correction method*

Empirical Quantile Mapping (EQM) downscaling is a method to bias correct data and its performance is well-established compared to other methods (Maurer *et al.*, 2010, Thrasher *et al.*, 2012, Bürger *et al.*, 2012). Mishra *et al.*, (2020b) used this statistical bias-correction method to remove the systematic biases inherent in the data. EQM is used to statistically downscale the bias-corrected daily maximum temperature and precipitation gridded data to the local and regional scale from a local set of observations. Gridded 0.25 degree ground-based observations of the variables are available for the years 1901-2018 and are obtained from the IMD as documented by Pai *et al.* (2014) and Sheffield *et al.* (2006) however Mishra *et al.* (2020 a, b) only used the period 1951-2014 to develop the cdfs and transfer functions. Bias-corrected maximum temperature and precipitation outputs from the historical period using the 0.25 degree gridded outputs are compared across the 13 GCMs from CMIP6 scenarios including Shared Socioeconomic Pathways (SSP), SSP126, SSP245, SSP370 and SSP585 scenarios for the 2015-2100 time periods. Mishra *et al.* (2020b) found that EQM successfully corrected the biases in the GCM

datasets including mean and extreme precipitation and minimum and maximum temperature. Since Mishra *et al.,* (2020a, b) already validated the EQM procedure, we do not reproduce the validation procedure here, and instead focus on the analysis and interpretation of results applied to the Bengal study region for assessing desertification.

EQM is a method to bias-correct and statistically downscale GCM datasets. Output time series of the variables including maximum temperature and precipitation were obtained from CMIP6 GCMs and exhibit inherent biases. Because of this inherent bias, these outputs need to be bias-corrected to produce topographically and regionally appropriate estimates at local scales for climate change assessment for decision-making. To achieve bias-correction, statistical transformations using cumulative distribution functions (cdfs) are used to map the model output (x_m) to the cdf of the observations (x_o) to produce bias-corrected model values (x^o_m). In general, this transformation can be formulated as Eq.1 (Piani *et al.*, 2010; Boé *et al.*, 2007) where we attempt to find some function *f* to do the transformation. The cdfs (F_o and F_m) of x_o and x_m are known in this case:

$$x^o_m = f(x_m) \qquad (1)$$

$$cdf(x_m) = F_m(x_m) \qquad (2)$$

$$cdf(x_o) = F_o(x_o) \qquad (3)$$

where, x^o_m is the bias-corrected model output, x_m is the model data from the GCM, x_o is the observations, and F_m and F_o are the Cumulative Distribution Functions (CDFs) of x_m and x_o respectively (Eq. 2 and Eq. 3). If the statistical distribution of x_m and x_o are known (F_o and F_m), the transformation *f* can be written as Eq. 4 where we estimate the bias-corrected output by matching the cdf of the model output (Eq. 2) to the cdf of the observations (Eq. 3):

$$x^o_m = F^{-1}_o(Fm (x_m)) \qquad (4)$$

Equation 4 maps the model outputs to the cdf of the observations providing bias-corrected model output. Once the cdfs are found, Eq. 4 can also be applied to projected climate data which exists in the absence of observations.

3.3. *Spatial Interpolation method*

All gridded data was mapped onto point (station) scales based on latitude and longitude using the Arc-GIS platform. Additionally, across the region, 84 stations were used to conduct an Inverse Distance Weighted interpolation (IDW) analysis and 43 of those stations fall directly within the study area. One of the best spatial interpolation methods is IDW (Das *et al.*, 2017) which predicts unknown values in areas based on known points. IDW is conducted in the Arc-GIS platform. For all data analysis, we used various software like SPSS and MS Excel.

3.4. *Data validation*

While Mishra *et al.* (2020b) already describe the validation details, we provide a brief overview here. Daily temporal resolution projections of maximum temperature and precipitation were bias corrected for the entire period of available GCM data (1951-2100). For the purposes of our study, we only consider the time period (2015-2041) for analysis, even though a longer projected time series is available. This method of data validation begins by first estimating the projected changes of mean annual precipitation and temperature using the raw data from the CMIP6-GCM. The projected changes were calculated from the GCMs for the late 21st century and analyzed alongside the historical reference period (1985-2014). Then, the multimodal ensemble mean of the projected changes from CMIP6-GCMs was calculated. After the multimodal ensemble mean is calculated for the 21st century projections, then the bias correction method is applied using the transform functions obtained for the period 1951-2014. Therefore, bias-corrected precipitation and temperature data was used for the historical (1951-2014) and future (2015-2041) periods. Finally, the uncertainty CMIP6-GCM data for mean annual precipitation, maximum and minimum temperatures were assessed against the observations from IMD (see Mishra *et al.* (2020 a, b)). Validation for the historical period (1985-2014) between observations and CMIP6-GCM data was conducted for the maximum and minimum temperatures and precipitation. Validation is conducted by comparing the mean seasonal cycle between the observations (1985-2014) and the CMIP6-GCM bias-corrected data for the historical period (1985-2014) and the level of uncertainty is quantified using one standard deviation confidence interval for the average seasonal cycle. Mishra *et al.* (2020b) found that the seasonal cycle, and the co-variability of precipitation and temperature compared well between the observations and CMIP6-GCM data which is a successful demonstration of EQM for bias-correcting data. Mishra *et al.*, 2020b also have shown that the transform functions are effective in reducing biases over the validation period of 1985-2014.

Statistical significance of the trends for precipitation and temperature are analyzed by decade (2022-2030 and 2031-2041) for all grid cells over the Bengal region by conducting a Kruskall-Wallis test. The Kruskall-Wallis test is a rank – based non - parametric alternative to the
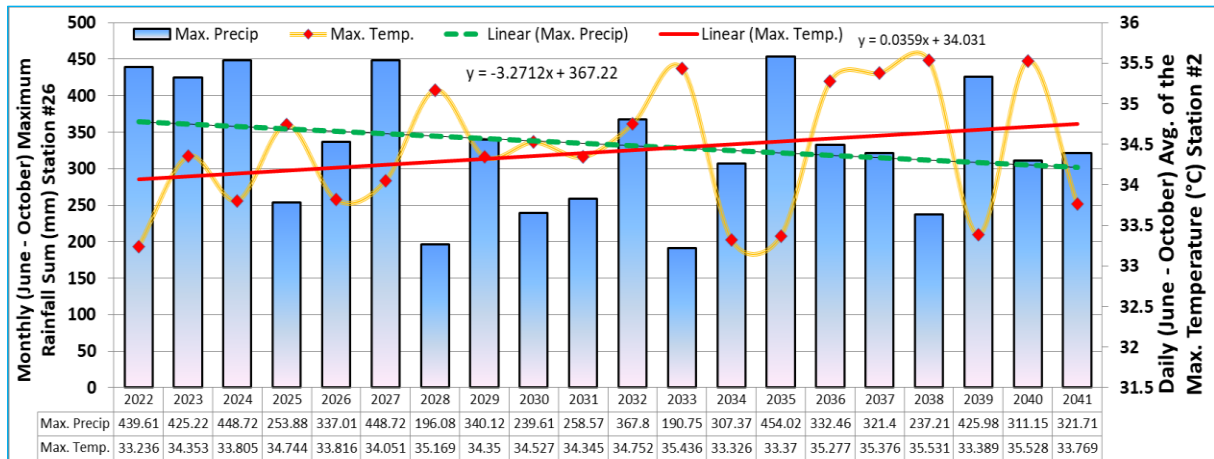
Fig. 2. Bar & Line graph for the monthly projected maximum precipitation and temperature data from 2022-2041. Bar graph represents the summation of the monsoonal rainfall (mm) monthly average for grid cell associated with station ID #26. The linear trend for precipitation is shown in green. The yellow line graph represents the daily average maximum temperature (^{0}C) with the linear trend line shown in red for grid cell associated with station ID #2.
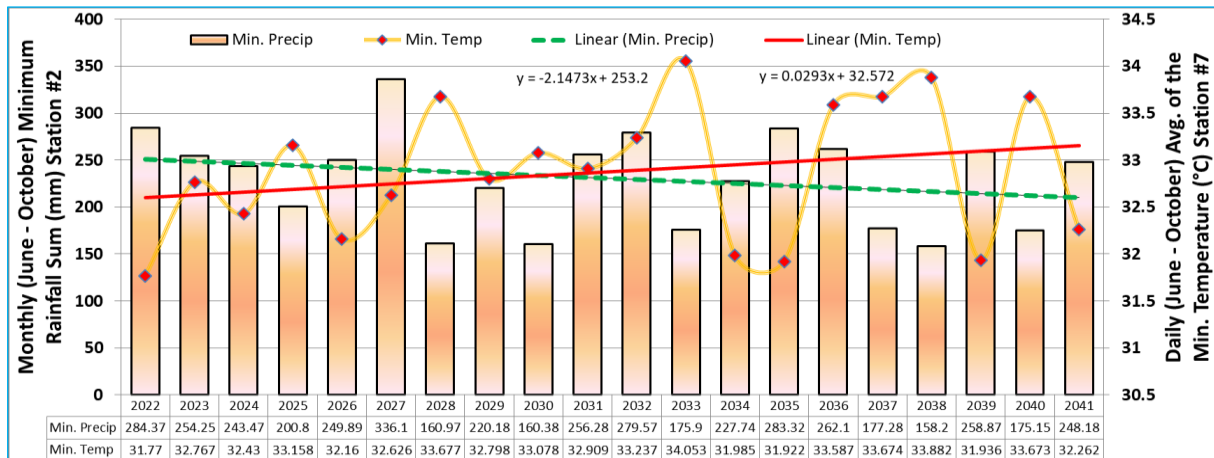

Fig. 3. Bar and Line graph for the monthly projected minimum precipitation and temperature data from 2022-2041. Bar graph represents the summation of the lowest value of monsoonal precipitation (mm) monthly minimums for grid cell associated with station ID #2. The linear trend is shown in green. The yellow line graph represents the minimum temperature (^{0}C) with the linear trend line shown in red for the grid cell associated with station ID #7.

ANOVA test that is used to determine if there are statistically significant differences between two or more groups. The Kruskall-Wallis test determines if the groups have the same mean on ranks and the statistical significance between the groups. We split the data up by the first decade 2022-2030 and second decade 2031-2041 and included all Bengal region spatial grid cells for temperature and precipitation in the grouping.

4. Results and discussion

4.1. *Climatic change and trend analysis (2022-2041)*

Bias-corrected future maximum temperature and precipitation projections for two decades (20 years) are shown annually (maximums Fig. 2 and minimums Fig. 3) and a table of values are provided in Supplementary Tables S1 (temperature) and S2 (precipitation). We

averaged and summed daily projected precipitation and temperature for the monsoon period (June - October). The daily average temperature and monthly average period for rainfall was assessed from the trend analysis shown in Figs. 2 and 3. The data in Figs. 2 and 3 represent spatial averages from the respective grid cells: for the precipitation and temperature maximums (Fig. 2), the spatial average is conducted for grid cells associated with station ID #2 and #26 respectively. For the precipitation and temperature minimums (Fig. 3), the spatial average is conducted for the grid cells associated with station ID #2 and #7 respectively. Monthly average monsoon precipitation decreases during the first two decades (2021-2041) at the station with the largest initial precipitation (station ID #26, 439.6 mm, initial year 2022) and declines by 117.9 mm over the 20 year period. At station ID #2, precipitation declines by 36.1 mm over the two decades. Average precipitation and temperature values during the

TABLE 1

Decadal Monsoon Climatic Variation (June to October) 2022-2041

S.ID	Longitude	Latitude	Maximum Temperature (ºC) Monthly			Rainfall (mm) Monsoon period		
			2022-2031	2032-2041	Δ2022-2041	2022-2031	2032-2041	Δ2022-2041
1	85.875	23.125	34.09	34.42	0.33	249.70	236.27	-13.43
2	85.875	23.375	34.24	34.58	0.34	236.67	224.63	-12.04
3	86.125	23.125	33.15	33.48	0.33	256.27	244.23	-12.04
4	86.125	23.375	33.27	33.62	0.35	253.42	241.21	-12.22
5	86.375	23.125	33.02	33.36	0.34	262.80	251.59	-11.21
6	86.375	23.375	32.85	33.21	0.36	259.77	248.02	-11.75
7	86.625	22.625	32.74	33.02	0.28	271.37	264.38	-6.99
8	86.625	22.875	32.77	33.08	0.31	270.65	261.52	-9.12
9	86.625	23.125	32.86	33.20	0.34	272.27	262.10	-10.17
10	86.625	23.375	33.16	33.53	0.37	267.30	256.56	-10.75
11	86.625	23.625	33.51	33.91	0.40	262.80	251.84	-10.96
12	86.875	22.125	33.03	33.30	0.27	305.30	299.72	-5.58
13	86.875	22.375	33.12	33.38	0.27	290.53	285.13	-5.40
14	86.875	22.625	32.98	33.26	0.28	283.27	276.32	-6.95
15	86.875	22.875	32.79	33.10	0.31	274.14	266.30	-7.84
16	86.875	23.125	33.02	33.36	0.34	268.64	260.89	-7.75
17	86.875	23.375	33.15	33.52	0.37	263.68	256.12	-7.55
18	86.875	23.625	33.52	33.92	0.41	263.86	255.63	-8.24
19	87.125	22.125	33.17	33.44	0.27	311.77	304.82	-6.95
20	87.125	22.375	32.78	33.04	0.26	299.40	293.57	-5.83
21	87.125	22.625	32.63	32.91	0.27	287.54	281.56	-5.97
22	87.125	22.875	32.97	33.28	0.31	270.66	264.95	-5.71
23	87.125	23.125	33.00	33.35	0.34	260.09	255.18	-4.91
24	87.125	23.375	33.23	33.60	0.38	256.86	252.31	-4.55
25	87.125	23.625	33.42	33.83	0.41	268.63	262.73	-5.90
26	87.375	21.875	33.53	33.84	0.31	338.75	326.99	-11.77
27	87.375	22.125	33.19	33.47	0.28	321.71	312.69	-9.02
28	87.375	22.375	32.80	33.05	0.26	302.88	296.34	-6.55
29	87.375	22.625	32.66	32.92	0.26	289.78	285.14	-4.64
30	87.375	22.875	33.05	33.35	0.30	275.16	271.58	-3.58
31	87.375	23.125	33.24	33.59	0.35	265.60	262.79	-2.82
32	87.375	23.375	33.33	33.71	0.38	265.21	262.63	-2.57
33	87.375	23.625	33.34	33.75	0.41	270.81	267.91	-2.91
34	87.375	23.875	33.53	33.96	0.43	278.69	273.33	-5.35
35	87.625	22.125	33.18	33.47	0.29	334.90	325.72	-9.18
36	87.625	22.625	32.75	33.02	0.27	295.71	291.31	-4.40
37	87.625	23.125	33.12	33.46	0.34	276.34	273.51	-2.83
38	87.625	23.625	33.41	33.83	0.42	267.35	264.57	-2.78
39	87.625	23.875	33.44	33.87	0.43	268.24	262.07	-6.17
40	87.625	24.125	33.55	33.99	0.44	277.57	268.50	-9.07
41	87.875	23.625	33.42	33.83	0.42	263.57	258.57	-5.00
42	87.875	24.125	33.63	34.08	0.44	273.26	262.68	-10.58
43	87.875	24.375	33.69	34.15	0.46	272.19	258.84	-13.34

TABLE S1

Daily Average Maximum Temperature during the Monsoon period (June-October) (°C) from 2022-2031 and 2032-2041

(a)

S. ID	Longitude	Latitude	2022	2023	2024	2025	2026	2027	2028	2029	2030	2031
1	85.875	23.125	33.08	34.21	33.69	34.56	33.67	33.91	35.05	34.22	34.36	34.19
2	85.875	23.375	33.24	34.35	33.81	34.74	33.82	34.05	35.17	34.35	34.53	34.35
3	86.125	23.125	32.16	33.25	32.72	33.62	32.67	32.99	34.09	33.24	33.45	33.29
4	86.125	23.375	32.31	33.36	32.80	33.76	32.79	33.12	34.18	33.35	33.60	33.43
5	86.375	23.125	32.06	33.09	32.58	33.49	32.48	32.89	33.95	33.08	33.37	33.21
6	86.375	23.375	31.93	32.92	32.34	33.33	32.31	32.73	33.75	32.89	33.22	33.07
7	86.625	22.625	31.77	32.77	32.43	33.16	32.16	32.63	33.68	32.80	33.08	32.91
8	86.625	22.875	31.85	32.81	32.39	33.19	32.20	32.67	33.67	32.81	33.14	32.97
9	86.625	23.125	31.97	32.91	32.41	33.30	32.28	32.77	33.75	32.88	33.26	33.10
10	86.625	23.375	32.28	33.21	32.62	33.63	32.56	33.08	34.05	33.15	33.59	33.43
11	86.625	23.625	32.67	33.59	32.94	33.96	32.93	33.43	34.35	33.46	33.92	33.82
12	86.875	22.125	32.16	33.00	32.81	33.41	32.53	32.90	33.96	33.14	33.25	33.16
13	86.875	22.375	32.24	33.09	32.87	33.50	32.54	33.01	34.03	33.17	33.44	33.30
14	86.875	22.625	32.10	32.96	32.68	33.37	32.36	32.88	33.88	32.99	33.37	33.20
15	86.875	22.875	31.94	32.79	32.41	33.18	32.16	32.71	33.66	32.77	33.21	33.03
16	86.875	23.125	32.19	33.05	32.56	33.43	32.39	32.96	33.88	32.97	33.48	33.30
17	86.875	23.375	32.34	33.20	32.60	33.57	32.50	33.10	33.99	33.06	33.64	33.46
18	86.875	23.625	32.75	33.60	32.92	33.92	32.90	33.48	34.32	33.39	34.00	33.87
19	87.125	22.125	32.41	33.09	32.96	33.50	32.65	33.04	34.04	33.24	33.42	33.34
20	87.125	22.375	32.02	32.70	32.54	33.11	32.19	32.66	33.63	32.80	33.13	33.00
21	87.125	22.625	31.88	32.57	32.34	32.98	32.00	32.53	33.48	32.61	33.06	32.89
22	87.125	22.875	32.22	32.94	32.60	33.34	32.32	32.90	33.81	32.91	33.44	33.26
23	87.125	23.125	32.25	33.01	32.53	33.38	32.33	32.96	33.83	32.89	33.52	33.32
24	87.125	23.375	32.49	33.27	32.67	33.61	32.54	33.21	34.04	33.07	33.78	33.58
25	87.125	23.625	32.72	33.51	32.81	33.78	32.76	33.41	34.18	33.22	33.97	33.80
26	87.375	21.875	32.85	33.40	33.38	33.82	33.05	33.36	34.44	33.66	33.68	33.67
27	87.375	22.125	32.52	33.07	32.99	33.49	32.62	33.06	34.04	33.24	33.46	33.40
28	87.375	22.375	32.14	32.68	32.56	33.10	32.17	32.68	33.61	32.79	33.18	33.07
29	87.375	22.625	32.02	32.55	32.38	32.96	32.02	32.56	33.45	32.60	33.11	32.96
30	87.375	22.875	32.38	32.99	32.67	33.39	32.36	32.99	33.86	32.93	33.56	33.37
31	87.375	23.125	32.55	33.23	32.76	33.60	32.51	33.23	34.05	33.07	33.81	33.61
32	87.375	23.375	32.65	33.37	32.76	33.69	32.59	33.34	34.11	33.11	33.96	33.73
33	87.375	23.625	32.70	33.43	32.72	33.66	32.64	33.35	34.06	33.08	33.96	33.76
34	87.375	23.875	32.94	33.69	32.91	33.79	32.91	33.54	34.18	33.26	34.09	33.97
35	87.625	22.125	32.59	33.06	33.00	33.45	32.58	33.07	34.00	33.20	33.45	33.40
36	87.625	22.625	32.17	32.64	32.48	33.03	32.07	32.67	33.51	32.64	33.19	33.05
37	87.625	23.125	32.53	33.11	32.65	33.43	32.38	33.12	33.86	32.90	33.71	33.47
38	87.625	23.625	32.84	33.52	32.79	33.70	32.67	33.46	34.08	33.10	34.08	33.83
39	87.625	23.875	32.94	33.61	32.83	33.65	32.80	33.47	34.03	33.14	34.04	33.87
40	87.625	24.125	33.12	33.78	32.94	33.68	32.99	33.56	34.06	33.26	34.08	33.99
41	87.875	23.625	32.96	33.55	32.83	33.67	32.67	33.49	34.01	33.08	34.13	33.79
42	87.875	24.125	33.29	33.88	33.04	33.74	33.05	33.67	34.09	33.33	34.20	34.03
43	87.875	24.375	33.40	34.00	33.09	33.72	33.18	33.72	34.08	33.42	34.19	34.10

(b)

S. ID	Longitude	Latitude	2032	2033	2034	2035	2036	2037	2038	2039	2040	2041
1	85.875	23.125	34.62	35.30	33.19	33.22	35.11	35.18	35.36	33.28	35.35	33.60
2	85.875	23.375	34.75	35.44	33.33	33.37	35.28	35.38	35.53	33.39	35.53	33.77
3	86.125	23.125	33.68	34.38	32.29	32.31	34.15	34.26	34.41	32.31	34.33	32.67
4	86.125	23.375	33.79	34.48	32.41	32.45	34.31	34.45	34.56	32.41	34.49	32.82
5	86.375	23.125	33.55	34.28	32.21	32.21	34.01	34.15	34.28	32.15	34.14	32.57
6	86.375	23.375	33.38	34.08	32.04	32.08	33.89	34.06	34.14	31.98	34.01	32.42
7	86.625	22.625	33.24	34.05	31.98	31.92	33.59	33.67	33.88	31.94	33.67	32.26
8	86.625	22.875	33.27	34.03	32.02	32.00	33.66	33.82	33.93	31.97	33.74	32.32

TABLE S1, (b) (*Conti.*)

S. ID	Longitude	Latitude	2032	2033	2034	2035	2036	2037	2038	2039	2040	2041
9	86.625	23.125	33.37	34.11	32.10	32.13	33.83	34.03	34.07	32.04	33.90	32.45
10	86.625	23.375	33.67	34.42	32.37	32.42	34.21	34.45	34.45	32.28	34.28	32.78
11	86.625	23.625	34.04	34.77	32.74	32.82	34.58	34.90	34.80	32.65	34.65	33.15
12	86.875	22.125	33.49	34.29	32.39	32.29	33.76	33.73	34.00	32.47	33.99	32.59
13	86.875	22.375	33.57	34.39	32.44	32.37	33.86	33.91	34.15	32.46	34.02	32.67
14	86.875	22.625	33.43	34.26	32.27	32.23	33.77	33.89	34.06	32.25	33.88	32.55
15	86.875	22.875	33.24	34.04	32.07	32.07	33.64	33.84	33.90	32.03	33.73	32.39
16	86.875	23.125	33.48	34.28	32.28	32.32	33.96	34.22	34.18	32.23	34.02	32.66
17	86.875	23.375	33.60	34.40	32.39	32.46	34.17	34.49	34.35	32.31	34.20	32.83
18	86.875	23.625	34.00	34.77	32.77	32.89	34.57	34.98	34.73	32.70	34.60	33.21
19	87.125	22.125	33.59	34.37	32.57	32.53	33.83	33.83	34.08	32.69	34.12	32.79
20	87.125	22.375	33.19	33.98	32.16	32.13	33.44	33.51	33.73	32.22	33.64	32.40
21	87.125	22.625	33.04	33.83	31.99	31.99	33.33	33.49	33.63	32.01	33.49	32.26
22	87.125	22.875	33.38	34.20	32.29	32.33	33.77	34.01	34.02	32.29	33.88	32.63
23	87.125	23.125	33.41	34.25	32.29	32.36	33.90	34.23	34.11	32.26	33.96	32.69
24	87.125	23.375	33.63	34.47	32.50	32.60	34.22	34.61	34.37	32.44	34.23	32.96
25	87.125	23.625	33.85	34.66	32.69	32.85	34.45	34.93	34.56	32.64	34.45	33.17
26	87.375	21.875	33.93	34.77	32.98	32.94	34.16	34.10	34.40	33.21	34.66	33.22
27	87.375	22.125	33.57	34.38	32.62	32.61	33.80	33.83	34.08	32.77	34.15	32.87
28	87.375	22.375	33.16	33.94	32.22	32.23	33.39	33.50	33.69	32.31	33.63	32.47
29	87.375	22.625	33.01	33.79	32.07	32.10	33.27	33.48	33.57	32.11	33.46	32.35
30	87.375	22.875	33.41	34.25	32.40	32.45	33.79	34.08	34.05	32.41	33.92	32.76
31	87.375	23.125	33.61	34.50	32.54	32.63	34.12	34.49	34.32	32.52	34.17	32.98
32	87.375	23.375	33.69	34.59	32.61	32.75	34.32	34.76	34.43	32.56	34.30	33.12
33	87.375	23.625	33.72	34.59	32.63	32.82	34.35	34.91	34.42	32.58	34.32	33.16
34	87.375	23.875	33.97	34.78	32.85	33.09	34.49	35.19	34.57	32.83	34.50	33.34
35	87.625	22.125	33.54	34.37	32.62	32.65	33.78	33.83	34.07	32.80	34.16	32.91
36	87.625	22.625	33.08	33.89	32.14	32.21	33.35	33.59	33.66	32.22	33.55	32.47
37	87.625	23.125	33.45	34.33	32.44	32.58	33.94	34.35	34.11	32.45	34.00	32.90
38	87.625	23.625	33.75	34.70	32.69	32.92	34.42	35.06	34.45	32.66	34.37	33.27
39	87.625	23.875	33.84	34.66	32.78	33.07	34.36	35.13	34.40	32.79	34.37	33.28
40	87.625	24.125	34.00	34.72	32.93	33.28	34.40	35.31	34.44	32.98	34.46	33.37
41	87.875	23.625	33.74	34.68	32.69	33.01	34.39	35.10	34.37	32.73	34.35	33.28
42	87.875	24.125	34.05	34.80	33.00	33.41	34.46	35.46	34.48	33.09	34.53	33.47
43	87.875	24.375	34.15	34.83	33.09	33.55	34.45	35.60	34.49	33.21	34.59	33.51

TABLE S2

Monsoon Rainfall Totals (June-October) of Bengal Dryland areas from 2022-2031 and 2032-2041 (mm)

(a)

S. ID	Longitude	Latitude	2022	2023	2024	2025	2026	2027	2028	2029	2030	2031
1	85.875	23.125	304.906	263.944	259.122	208.892	260.872	368.728	162.918	233.372	169.956	264.25
2	85.875	23.375	284.374	254.248	243.472	200.796	249.888	336.104	160.974	220.18	160.378	256.284
3	86.125	23.125	308.816	280.508	268.204	211.026	276.2	365.652	165.334	247.28	172.074	267.616
4	86.125	23.375	308.708	282.908	262.01	209.406	276.496	364.454	161.65	238.772	164.848	264.96
5	86.375	23.125	313.112	292.442	275.998	215.146	289.342	360.778	171.956	260.254	179.956	269.03
6	86.375	23.375	316.062	297.846	269.032	213.718	288.094	358.578	166.034	251.652	171.538	265.172
7	86.625	22.625	319.934	281.506	295.422	218.704	288.204	383.828	186.82	279.06	195.204	265.022
8	86.625	22.875	323.098	293.996	291.16	216.04	296.83	379.898	176.762	277.136	185.328	266.216
9	86.625	23.125	330.392	309.368	289.018	216.412	307.626	381.394	167.966	276.166	175.886	268.446
10	86.625	23.375	322.182	313.612	280.02	217.68	307.156	359.692	165.484	269.13	171.546	266.506
11	86.625	23.625	311.862	313.194	276.02	216.256	305.298	345.274	160.066	269.306	168.018	262.71
12	86.875	22.125	380.964	338.668	357.594	241.698	307.25	428.672	193.19	308.338	221.956	274.714
13	86.875	22.375	352.458	313.202	333.186	226.46	302.41	430.308	182.4	303.848	198.17	262.866
14	86.875	22.625	336.184	304.604	312.518	225.996	304.954	403.832	188.22	298.512	193.41	264.438
15	86.875	22.875	327.93	304.66	297.294	220.28	303.02	378.412	180.934	287.34	182.936	258.63

S. ID	Longitude	Latitude	2022	2023	2024	2025	2026	2027	2028	2029	2030	2031
						TABLE S2, (a) *(Conti.)*						
16	86.875	23.125	326.648	309.262	288.958	214.754	307.978	368.472	168.036	280.942	168.342	252.986
17	86.875	23.375	321.516	310.088	279.948	215.542	309.39	346.794	164.954	273.748	163.338	251.438
18	86.875	23.625	315.894	309.502	280.916	220.816	309.048	334.318	170.32	276.878	168.24	252.7
19	87.125	22.125	389.726	359.748	378.174	243.644	316.684	429.056	195.514	320.168	220.622	264.368
20	87.125	22.375	365.922	339.382	350.07	232.2	313.02	440.106	185.012	318.526	195.662	254.09
21	87.125	22.625	342.742	319.758	320.602	230.598	311.562	404.496	191.202	309.03	189.622	255.74
22	87.125	22.875	320.746	304.468	297.176	221.188	302.072	360.226	184.182	290.89	179.316	246.344
23	87.125	23.125	314.512	300.264	283.122	212.15	302.494	341.05	169.854	279.294	162.61	235.52
24	87.125	23.375	312.036	301.072	276.702	212.82	307.504	324.886	166.158	276.222	156.68	234.502
25	87.125	23.625	323.44	313.108	290.49	226.448	321.55	329.54	178.338	291.736	165.978	245.68
26	87.375	21.875	439.612	425.216	448.722	253.878	337.012	448.72	196.082	340.116	239.606	258.566
27	87.375	22.125	399.972	385.188	394.572	252.064	328.578	432.298	205.292	330.996	227.132	261.05
28	87.375	22.375	364.464	350.17	353.25	241.884	318.158	417.318	201.178	324.276	204.11	254.032
29	87.375	22.625	343.412	329.834	326.732	235.22	316.304	395.182	197.172	316.968	188.604	248.362
30	87.375	22.875	326.632	316.074	307.816	226.018	312.38	360.736	187.862	301.33	175.074	237.69
31	87.375	23.125	317.568	307.99	294.468	220.468	312.964	334.312	180.552	292.452	163.9	231.368
32	87.375	23.375	318.888	309.108	291.732	223.524	322.128	318.894	180.488	294.892	159.706	232.692
33	87.375	23.625	322.116	314.906	301.418	230.988	334.538	317.268	183.796	305.814	160.308	236.962
34	87.375	23.875	324.888	319.054	317.564	242.676	337.068	319.64	194.846	322.254	168.046	240.834
35	87.625	22.125	407.514	408.196	422.152	259.9	346.918	438.962	213.648	356.682	233.33	261.676
36	87.625	22.625	345.154	340.432	339.55	236.674	328.668	400.958	201.914	338.48	183.544	241.686
37	87.625	23.125	321.62	317.528	308.78	229.814	334.116	336.796	196.144	317.548	167.56	233.486
38	87.625	23.625	306.058	305.72	300.552	230.132	339.698	299.666	195.622	309.634	158.606	227.826
39	87.625	23.875	298.634	300.584	311.888	237.024	336.396	293.154	202.316	315.336	161.44	225.596
40	87.625	24.125	301.314	308.706	335.42	248.652	346.658	296.282	213.474	333.642	163.874	227.672
41	87.875	23.625	286.702	292.774	295.558	225.604	346.452	290.61	207.384	314.308	155.154	221.11
42	87.875	24.125	280.342	298.932	339.054	246.732	362.458	284.802	224.05	335.102	147.486	213.594
43	87.875	24.375	271.948	287.266	350.612	257.144	356.302	273.9	232.268	327.35	152.494	212.572

(b)

S. ID	Longitude	Latitude	2032	2033	2034	2035	2036	2037	2038	2039	2040	2041
1	85.875	23.125	299.262	173.132	232.764	296.372	276.614	199.264	165.892	273.552	188.436	257.406
2	85.875	23.375	279.566	175.902	227.742	283.318	262.096	177.282	158.196	258.868	175.15	248.176
3	86.125	23.125	310.892	176.262	241.218	302.874	279.872	205.408	164.238	292.49	206.704	262.39
4	86.125	23.375	308.428	182.876	242.428	297.65	277.082	189.664	159.552	291.96	198.198	264.214
5	86.375	23.125	316.208	183.574	251.786	303.662	279.98	216.93	166.84	303.306	224.566	269.04
6	86.375	23.375	316.82	189.594	252.334	294.218	276.926	199.896	161.218	304.828	216.634	267.736
7	86.625	22.625	332.41	171.548	253.28	324.522	278.024	276.224	177.006	310.606	252.606	267.592
8	86.625	22.875	333.522	175.044	254.092	320.302	283.174	244.732	169.944	319.326	244.986	270.122
9	86.625	23.125	340.442	182.926	259.36	315.568	290.802	223.882	164.834	326.898	240.702	275.572
10	86.625	23.375	326.948	193.45	264.386	300.792	287.976	201.078	163.388	320.694	231.026	275.816
11	86.625	23.625	312.444	199.844	262.184	295.996	286.354	186.134	164.468	310.052	225.402	275.488
12	86.875	22.125	356.498	172.612	278.172	390.774	313.296	320.474	207.272	372.148	285.45	300.51
13	86.875	22.375	361.996	161.27	261.278	371.652	302.118	299.028	185.352	352.338	273.802	282.508
14	86.875	22.625	350.406	172.792	265.252	349.412	294.222	271.604	180.998	338.858	262.51	277.156
15	86.875	22.875	337.89	179.088	264.102	327.964	286.968	240.2	173.762	329.914	250.244	272.91
16	86.875	23.125	339.052	181.772	263.392	313.856	288.114	214.922	165.572	329.622	240.672	271.89
17	86.875	23.375	331.076	191.574	267.982	298.29	285.776	194.538	163.622	323.904	231.886	272.564
18	86.875	23.625	319.374	204.494	270.716	296.108	284.444	187.68	171.224	314.694	231.054	276.482
19	87.125	22.125	359.26	179.232	288.614	404.906	318.246	308.404	213.282	382.486	289.592	304.176
20	87.125	22.375	369.746	165.814	273.568	390.178	311.258	289.298	190.508	374.706	281.554	289.09
21	87.125	22.625	354.646	176.044	275.836	360.31	299.994	262.626	184.802	353.824	266.866	280.674
22	87.125	22.875	329.448	181.502	269.94	326.31	284.768	230.794	177.174	330.27	247.274	272.002
23	87.125	23.125	325.726	181.164	265.892	305.882	278.392	205.664	167.02	322.28	235.08	264.702
24	87.125	23.375	323.422	190.426	270.102	293.122	278.276	186.29	165.312	319.02	230.568	266.53
25	87.125	23.625	329.148	211.088	282.706	303.99	288.52	186.698	177.924	324.95	240.898	281.344

			TABLE S2, (b) *(Conti.)*									
S. ID	Longitude	Latitude	2032	2033	2034	2035	2036	2037	2038	2039	2040	2041
26	87.375	21.875	367.8	190.752	307.372	454.022	332.46	321.404	237.21	425.976	311.15	321.708
27	87.375	22.125	363.248	192.352	303.848	420.612	322.082	301.294	223.26	396.72	294.07	309.444
28	87.375	22.375	358.392	182.444	291.922	390.67	311.872	277.894	202.398	375.764	279.664	292.368
29	87.375	22.625	352.666	181.66	287	366.962	303.498	253.74	190.626	364.158	267.298	283.812
30	87.375	22.875	337.33	185.824	282.934	336.816	291.57	227.99	182.562	344.466	251.448	274.848
31	87.375	23.125	329.198	190.76	281.402	315.402	283.9	204.894	175.886	332.67	242.946	270.826
32	87.375	23.375	332.176	202.26	288.228	304.618	285.73	188.814	174.398	331.086	243.458	275.55
33	87.375	23.625	334.098	217.556	295.032	307.362	291.936	184.112	182.41	332.816	248.142	285.592
34	87.375	23.875	327.24	234.702	296.066	317.976	294.07	189.06	198.138	326.166	253.948	295.976
35	87.625	22.125	375.564	200.98	324.206	443.934	329.362	299.758	232.184	422.318	306.848	322.06
36	87.625	22.625	360.03	181.798	299.64	380.552	304.72	247.476	192.302	384.068	274.776	287.716
37	87.625	23.125	337.066	197.532	301.568	326.45	289.902	206.548	185.896	353.548	254.786	281.76
38	87.625	23.625	318.044	215.936	302.862	298.418	283.53	182.83	186.616	331.138	243.276	283.068
39	87.625	23.875	302.248	226	295.762	297.444	276.868	183.222	194.796	316.152	242.822	285.392
40	87.625	24.125	296.51	246.086	298.196	305.17	280.674	186.992	208.68	314.462	251.982	296.234
41	87.875	23.625	299.592	208.262	310.968	285.482	270.14	180.608	188.138	328.316	234.208	279.98
42	87.875	24.125	284.196	235.242	303.494	289.734	270.718	179.534	202.514	321.794	248.376	291.172
43	87.875	24.375	266.496	245.072	294.554	286.54	260.248	180.966	207.796	303.71	249.548	293.504
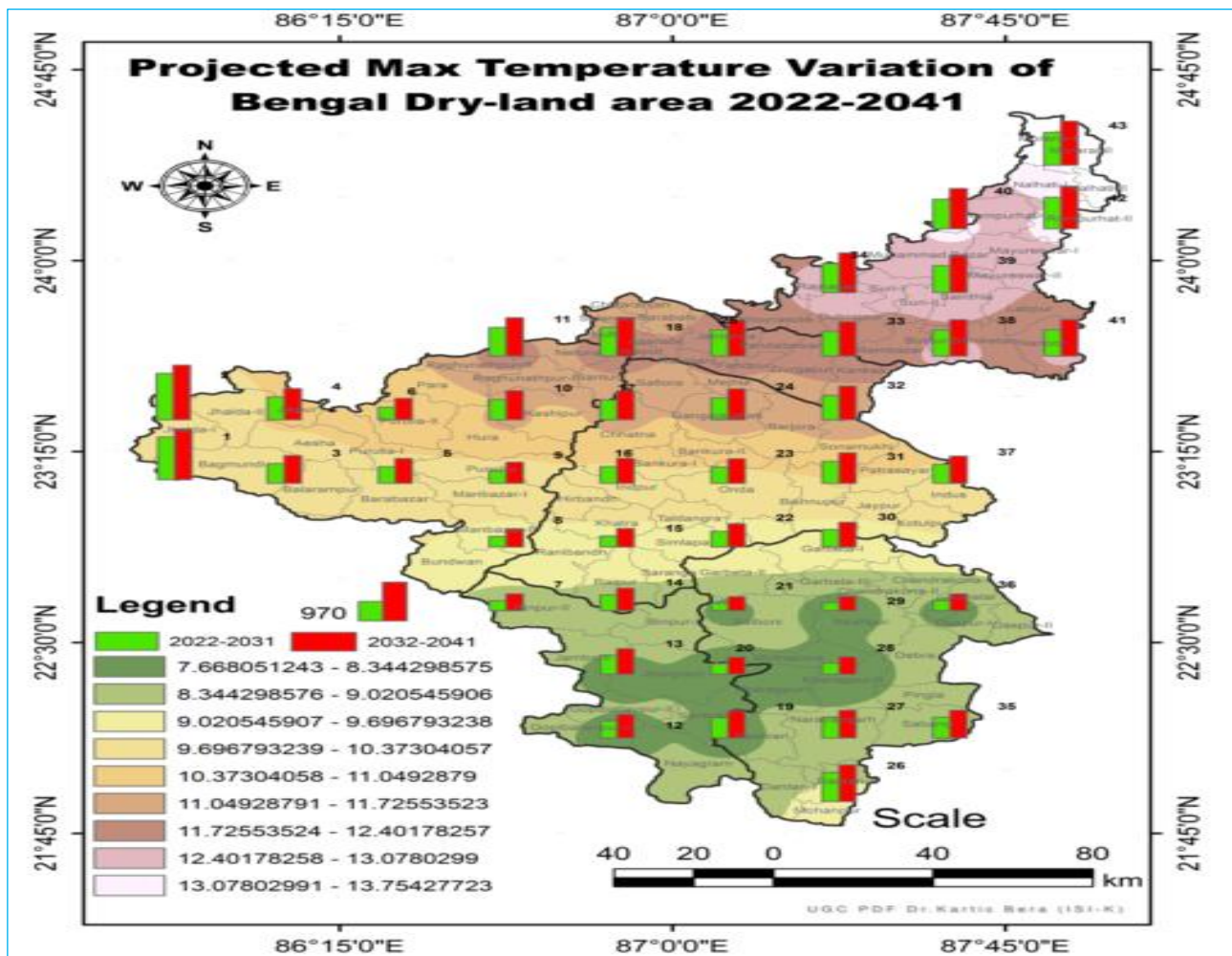
Fig. 4. Projected decadal (2022-2031) and (2032-2041) maximum temperature variations (+ indicates increases, and – indicates decreases) are shown. The IDW interpolated temperature variation values are mapped for the entire region. Green values indicate temperature rises between +7.6 to +9.2 °C and red/pink values indicate the higher temperature rises between +12.4 to +13.75 °C.
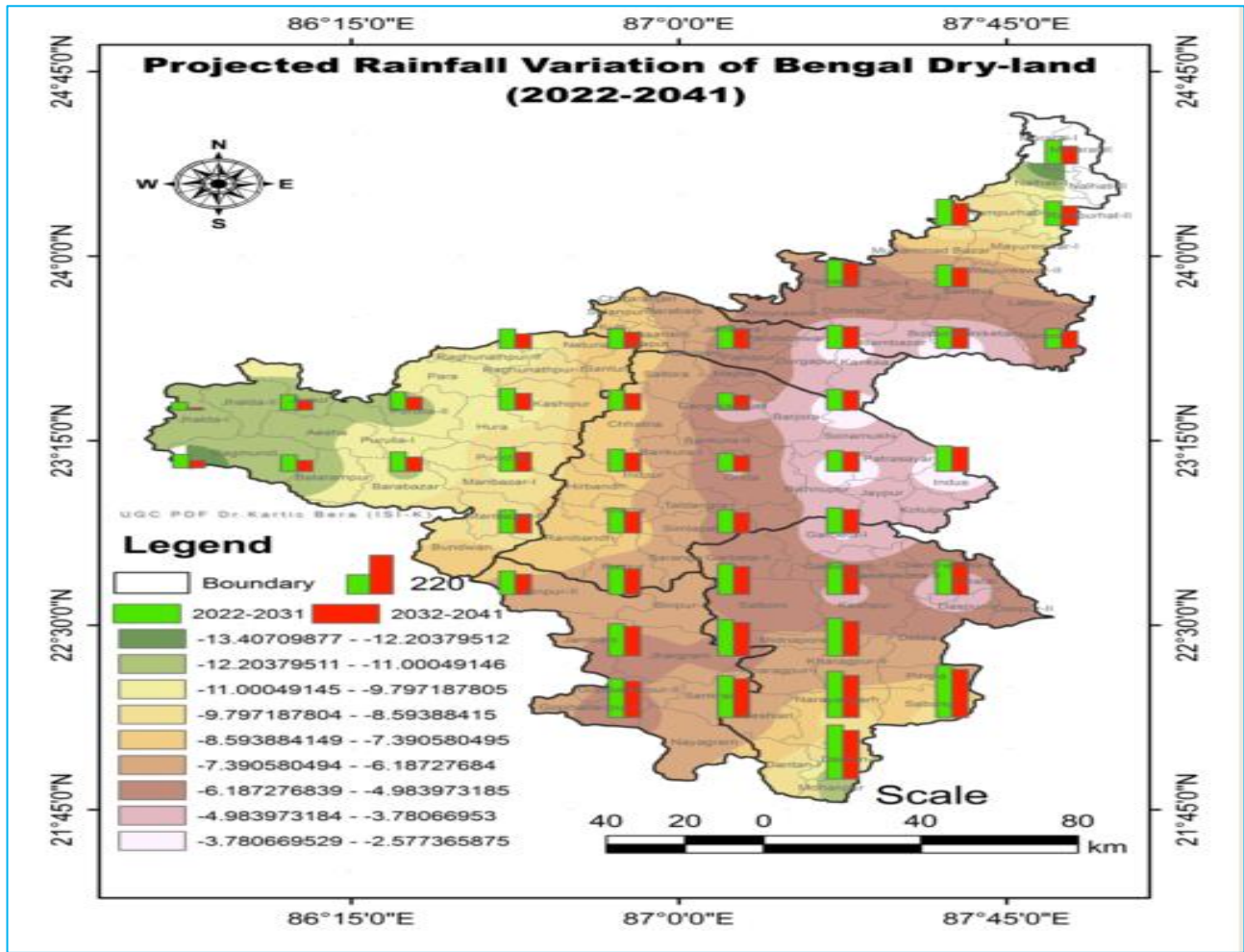
Fig. 5. Projected decadal (2022-2031) and (2032-2041) of precipitation variations (+ indicates increases and – indicates decreases) are shown. The IDW interpolated precipitation values are mapped for the entire region. Green values indicate larger magnitude decreases in precipitation (-13.4 to -12.2 mm), and pink/light pink values indicate the smallest magnitude decreases in precipitation (-3.7 to -2.5 mm).

monsoon period for each decade by station ID and average change values (Δ) are provided in Table 1. Station ID # 2, and Station ID #26 are highlighted because they represent the lowest and highest average precipitation for the region. The Kruskall-Wallis test for statistically significant differences indicates a significant negative difference in preci-pitation by decade at the p < 0.1 level (decade 2022-2030 versus 2031-2041, chi-squared = 3.2349, df = 1, p-value = 0.07209) when evaluated for the entire Bengal region .

Future maximum temperature gradually increases; in the first-decade, daily average maximum temperature across the entire region is 33.10 °C, whereas in the second decade the highest max-temperature is 33.50 °C (station ID #43) representing almost 0.5 degree °C rise in temperature. At station ID #26, the initial 2022 year temperature is 32.85 °C, and will increase by 3.823 °C

over the next two decades based on the linear trend. Over the two-decades of interest (2022-2041), temperature will increase between 0.1 °C - 0.5 °C (regression linear forecast lines, Figs. 2 and 3). The Kruskall-Wallis test for statistically significant differences indicates a significant positive difference in temperature by decade at the p << 0.01 level (decade 2022-2030 versus 2031-2041, chi-squared = 36.741, df = 1, p-value = 1.349e-09) when evaluated for the entire Bengal region.

Annual projected precipitation data shows a long-term declining change from 2022 to 2041. For the Bengal dryland region, the CMIP6-GCM shows a drying bias (15-20%) in mean annual rainfall. However, the multimodal ensemble mean annual precipitation is projected to slightly increase under the projected future climate over the entire sub-continent of India and the South Asia region (Mishra *et al.*, 2020b). While it is

common for GCM scenarios to widely vary with the SSP, the projected increase in precipitation under the multi-model ensemble mean of future climate varies with the scenario considered and does not represent local conditions. Given the wide ranging variability across the continent, we find that for the local Bengal dryland region, the climate will be warmer and dryer due to increasing temperature and decreasing rainfall contributing to possible future dryland expansion.

4.2. *Spatial analysis*

The interpolated thematic maps for precipitation and temperature variables are shown over the entire Bengal dryland region (Figs. 4 and 5). Spatially, we find regionally variable differences in projected monsoon temperature and precipitation. While the average values of climate variables are summarized by decade (2022-2031) and (2032-2041) in Table 1, spatially variable changes in temperature and precipitation are shown in the maps in Figs. 4 and 5. Fig. 4 shows the IDW constructed spatial variability in temperature change patterns by decade. Bar-graphs indicate point-scale data. Fig. 5 shows the IDW constructed spatial variability in precipitation change patterns by decade with bar-graphs similarly indicating point scale data. Spatially, temperature increases across the entire dryland region during the monsoon period (June to October), whereas rainfall decreases across the entire region albeit by slightly different magnitudes with rainfall decreasing the most in the eastern Bengal region (Fig. 5, Table 1). In the next two decades, the climatic environment of the dryland region will experience warming and reduced precipitation, contributing to potentially greater soil moisture deficits and evapotranspiration. Combined with a rapidly growing human population, these future climatic conditions will exacerbate the risk of land degradation and desertification (Huang *et al*., 2016).

5. Discussion and future work

Our research indicates that the Bengal dryland region will experience warmer and dryer future climate conditions which can exacerbate the potential for desertification. Our work finds that assessing dryland areas using bias-corrected data is consistent with observations for the climatological mean period and can be used to project future climate patterns for this region. Therefore, observational datasets will be critical to better predict future climate change and their implications in different sectors (*e.g*., water resources and agriculture). Also important are observations of precipitation and temperature that can be used to model recharge and groundwater storage potential in critically important arid regions of the world (Bera *et al*., 2022). Furthermore,

using validation data, novel techniques to conduct aquifer recharge site selection, and physically-based models, will be needed to consider the physical changes introduced under climate scenarios such as precipitation, temperature, biogeochemistry, and land-use changes in the next century (Newcomer *et al.*, 2014, Maina *et al.*, 2020, Maavara *et al.*, 2021). Our findings have important implications indicating potential desertification and designing sustainable development and land-use plans for the coming century in response to these changes will be of upmost importance. These climate change variables will be critically important when considering how to design land management strategies under future climate change.

6. Conclusion

Studies of climate change highlight the highly variable nature of temperature and precipitation projections in dryland regions. We find trends in monsoonal temperature and precipitation with increasing temperature (+0.1 to +0.5 °C) and decreasing precipitation (- 2 to -12 mm) observed over the next two decades at spatially variable rates across the Bengal region. These warming and drying trends in the study area are widening the gap between water demand and supply, hence the need for ways and solutions to capture and store needed water supplies. Additionally, the significance of these changes lie in the response of evapotranspiration and soil moisture, with previous work suggesting that even a small temperature increase of +5% can lead to 14% greater evapotranspiration (Goyal, 2004). Urgent steps need to be undertaken on both local and state levels to address the widening water availability gap. Some of the solutions would be new agricultural practices that require smaller quantities of water, rainwater harvesting, surface water utilization plans, managed aquifer recharge and the use of more eco-friendly energy in various economic sectors.

Disclaimer : The contents and views presented in this research article/paper are the views of the authors and do not necessarily reflect the views of the organizations they belong to.

References

Arora, B., Burrus, M., Newcomer, M. E., Steefel, C. I., Carroll, R. W. H., Dwivedi, D., Dong W., Willams K. H. and Hubbard, S. S., 2020, "Differential C-Q Analysis: A New Approach to Inferring Lateral Transport and Hydrologic Transients Within Multiple Reaches of a Mountainous Headwater Catchment", *Frontiers in Water*, **2**, 24. doi : https://doi.org/10.3389/frwa.2020.00024.

Bera, S. and Bera, K., 2014, "Geo-informatics Approach to Demarcate Ground Water Potential Zone in Semi-Arid Region of Kansai-Tangai Interfluves area", *International Multidisciplinary e-Journal,* **III**, IX, https://scholar.google.co.in/scholar? cluster= 10732452785 953863950 &hl=en&as_sdt=2005.

Bera, K., Newcomer, M. E. and Banik, P., 2022, "Groundwater recharges site suitability analysis through multi-influencing factors (MIF) in West Bengal dry-land areas, West Bengal, India", *Acta Geochimica*. doi : https://doi.org/10.1007/s11631-022-00559-6.

Boé, J., Terray, L., Habets, F. and Martin, E., 2007, "Statistical and dynamical downscaling of the Seine basin climate for hydro-meteorological studies", *International Journal of Climatology*, **27**, 12, 1643-1655. doi : https://doi.org/10.1002/joc.1602.

Brahim Y. A., Saidi M. E. M., Kouraiss K., Sifeddine A. and Bouchaou L., 2017, "Analysis of observed climate trends and high resolution scenarios for the 21st century in Morocco," p10.

Bürger, G., Murdock, T. Q., Werner, A. T., Sobie, S. R. and Cannon, A. J., 2012, "Downscaling extremes-an inter comparison of multiple statistical methods for present climate", *J. Clim*. **25**, 4366-4388, doi : doi.org/10.1175/JCLI-D-11-00408.1.

Census of India. Office of the Registrar General & Census Commissioner India, Ministry of Home Affairs, Government of India (2011), https://censusindia.gov.in/census.website/ data/census-tables.

Cheng, Y., Bhoot, V. N., Kumbier, K., Sison-Mangus, M. P., Brown, J. B., Kudela, R. and Newcomer, M. E., 2021, "A novel random forest approach to revealing interactions and controls on chlorophyll concentration and bacterial communities during coastal phytoplankton blooms. Scientific Reports", **11**, 1, 19944. doi : https://doi.org/10.1038/s41598-021-98110-9.

Das, M., A. Hazra, A. Sarkar, S. Bhattacharya, P. Banik., 2017, "Comparison of spatial interpolation methods for estimation of weekly rainfall in West Bengal, India", *MAUSAM*. **68**, 41-50. doi : 10.54302 /mausam.v68i1.407.

Enguehard, L., Falco, N., Schmutz, M., Newcomer, M. E., Ladau, J., Brown, J. B., Laura Bourgeau-Chavez, and Haruko M. Wainwright, 2022, "Machine-Learning Functional Zonation Approach for Characterizing Terrestrial-Aquatic Interfaces: Application to Lake Erie. Remote Sensing, **14**, 14, 3285. doi : https://doi.org/10.3390/rs14143285.

Goyal, R. K., 2004, "Sensitivity of evapotranspiration to global warming: a case study of arid zone of Rajasthan (India)", Agr. Water Manag., **69**, 1-11.   doi : https://doi.org/10.1016/j.agwat. 2004.03.014.

Herrmann, S. M., A. Anyamba, C. J. Tucker, 2005, "Recent trends in vegetation dynamics in the African Sahel and their relationship to climate Global Environmental Change-Human and Policy Dimensions", **15**, 394-404. doi : https://doi.org/10.1016/j. gloenvcha.2005.08.004.

Hofmann, T., Schölkopf, B. and Smola, A. J. Kernel, 2008 "methods in machine learning" *Ann. Stat*., 1171-1220.

Huang, J., Yu, H., Guan, X. Wang. G. and Guo, R., 2016, "Accelerated dryland expansion under climate change. *Nature Clim Change,* **6,** 166-171, doi : https://doi.org/10.1038/nclimate2837.

IPCC, 2007: Summary for Policymakers. In: Climate Change 2007: The Physical Science Basis. Contribution of Working Group I to the Fourth Assessment Report of the Intergovernmental Panel on Climate Change [Solomon, S., D. Qin, M. Manning, Z. Chen, M. Marquis, K.B. Averyt, M. Tignor and H. L. Miller (eds.)]. Cambridge University Press, Cambridge, United Kingdom and New York, NY, USA. https://www.ipcc.ch/site/ assets/uploads/2018/02/ar4-wg1-spm-1.pdf .

Jain, Sharad and Kumar, Vijay., 2012, "Trend analysis of rainfall and temperature data for India SK Jain, V Kumar", *Current Science* (Bangalore) **102** 1, 37-49. http://www.hpccc.gov.in/PDF/ Rainfall/Trends%20Analysis%20of%20Rainfall%20and%20Te mperature.pdf.

Kumar, V., Jain, S. K. and Singh, Y., 2010, "Analysis of long-term rainfall trends in India", *Hydrol. Sci. J*., **55**, 484-496.

Lal, M., 2001, "Climatic change - implications for India's water resources", *J. Indian Water Resour. Soc*., **21**, 101-119.

Lee, J., Kim, C. G., Lee, J. E., Kim, N. W. and Kim, H., 2018, "Application of Artificial Neural Networks to Rainfall Forecasting in the Geum River Basin", *Korea. Water* , **10**, 1448. doi : doi.org/10.3390/w10101448.

Maavara, T., Siirila-Woodburn, E. R., Maina, F., Maxwell, R. M., Sample, J. E., Chadwick, K. D., Rosemary Carroll, Michelle E. Newcomer, Wenming Dong, Kenneth H. Williams, Carl I. Steefel and Nicholas J. Bouskill, 2021, "Modeling geogenic and atmospheric nitrogen through the East River Watershed, Colorado Rocky Mountains", *PLOS ONE*, **16**, 3, e0247907. doi : https://doi.org/10.1371/journal.pone.0247907.

Maina, F. Z., Siirila-Woodburn, E. R., Newcomer, M. E., Xu, Z. and Steefel, C., 2020, "Determining the impact of a severe dry to wet transition on watershed hydrodynamics in California, USA with an integrated hydrologic model", *Journal of Hydrology*, **580**, 124358. doi : https://doi.org/10.1016/j.jhydrol.2019. 124358.

Matheus Carnevali, P. B., Lavy, A., Thomas, A. D., Crits-Christoph, A., Diamond, S., Méheust, R., Olm, R. M., Sharrar, A., Lei, S., Dong, W., Falco, N., Bouskill, N., Newcomer, E. M., Nico, P., Wainweight, H., Dwivedi, D., Williams, H. K., Hubbard, S. and Banfield, F. J., 2021, "Meanders as a scaling motif for understanding of floodplain soil microbiome and biogeochemical potential at the watershed scale. Microbiome, **9**, 1, 121. doi : https://doi.org/10.1186/s40168-020-00957-z.

Maurer, E. P., Hidalgo, H. G., Das, T., Dettinger, M. D. and Cayan, D. R., 2010, "The utility of daily large-scale climate data in the assessment of climate change impacts on daily streamflow in California. Hydrol", *Earth Syst. Sci*. **14**, 1125-1138, doi : doi.org/10.5194/hess-14-1125-2010.

Mishra, V., Aadhar, S., Asoka, A., Pai, S., and Kumar, R., 2016, "On the frequency of the 2015 monsoon season drought in the Indo-Gangetic Plain", *Geophysical Research Letters*, **43**, 23. doi : https://doi.org/10.1002/2016GL071407.

Mishra, V., Bhatia, U., and Tiwari, A. D., 2020a, "Bias Corrected Climate Projections from CMIP6 Models for South Asia [Data set]", *Zenodo*. doi : https://doi.org/10.5281/ZENODO. 3873028.

Mishra, V., Bhatia, U. and Tiwari, A. D., 2020b, "Bias-corrected climate projections for South Asia from Coupled Model Intercomparison Project-6. *Sci Data* **7,** 338, doi : doi.org/10. 1038/s41597-020-00681-1.

Mortimore, M. J., Anderson, S., Cotula, L., Davies, J., Faccer, K., Hesse, C., Morton, J. F., Nyangena, W., Skinner, J., and Wolfangel, C., 2009, "Dryland opportunities: a new paradigm for people", *ecosystems and development*. doi : https://pubs.iied.org/g02572.

Newcomer, M. E., Gurdak, J. J., Sklar, L. S. and Nanus, L., 2014, "Urban recharge beneath low impact development and effects of climate variability and change: recharge beneath low impact development and climate change", *Water Resources Research*, **50**, 2, 1716-1734. doi : https://doi.org/10.1002/2013WR014282.

Pai, D. S., Rajeevan, M., Sreejith, O. P., Mukhopadhyay, B. and Satbhai, N. S., 2014, "Development of a new high spatial resolution ($0.25° \times 0.25°$) long period (1901-2010) daily gridded rainfall data set over India and its comparison with existing data sets over the region. *MAUSAM*. 65, 1-18. doi : 10.54302/ mausam.v65i1.851.

Piani, C., Haerter, J. O. and Coppola, E., 2010, "Statistical bias correction for daily precipitation No index entries found. Regional climate models over Europe", *Theor. Appl. Climatol*. **99**, 187-192.

Rasmussen, C. E. and Williams, C. K. I. Gaussian processes for machine learning. (MIT Press, 2006).

Rath S, Panda J. and Sarkar A., 2022, "Distinct urban land cover response to meteorology in WRF simulated pre-monsoon thunderstorms over the tropical city of Kolkata", *Meteorology and Atmospheric Physics*., **134**. doi :10.1007/s00703-022-00916-3.

Rogers, D. B., Newcomer, M. E., Raberg, J. H., Dwivedi, D., Steefel, C., Bouskill, N., Nico, P., Faybishenko, B., Fox, P., Conrad, M., Bill, M., Brodie, E., Arora, B., Dafflon, B., Williams, H. K. and Hubbard, S. S., 2021, "Modeling the Impact of Riparian Hollows on River Corridor Nitrogen Exports", *Frontiers in Water*, **3**, 590314. doi : https://doi.org/10.3389/frwa.2021. 590314.

Sadhukhan I, Lohar D, Pal D. K., 2003, "Land use alterations and its possible impact on premonsoon climatic variables", *Journal of the Indian Society of Remote Sensing*, **31**, 261-269.

Sheffield, J., G. Goteti and E. F. Wood, 2006, "Development of a 50-Year High-Resolution Global Dataset of Meteorological Forcings for Land Surface Modeling", *J. Climate*, **19**, 3088-3111, doi : https://doi.org/10.1175/JCLI3790.1.

Singh, H. V., Joshi, N. and Suryavanshi, S., 2023, "Projected climate extremes over agro-climatic zones of Ganga River Basin under 1.5, 2 and 3° global warming levels", *Environmental Monitoring and Assessment*, **195**, 9, 1062. doi : https://doi.org/10.1007/s10661-023-11663-2.

Sinha Ray, K. C. and De, U. S., 2003, "Climate change in India as evidenced from instrumental records," *WMO Bull*., **52**, 53-59.

Sprenger, M., Carroll, R. W. H., Dennedy-Frank, J., Siirila-Woodburn, E. R., Newcomer, M. E., Brown, W., Newman, A., Beutler, C., Bill, M., Hubbard, S. S. and Williams, H. K., 2022, "Variability of Snow and Rainfall Partitioning Into Evapotranspiration and Summer Runoff Across Nine Mountainous Catchments", *Geophysical Research Letters,* **49**, 13. doi : https://doi.org/10. 1029/2022GL099324.

Thrasher, B., Maurer, E. P., McKellar, C. and Duffy, P. B., 2012, "Technical Note: Bias correcting climate model simulated daily temperature extremes with quantile mapping", *Hydrol. Earth Syst. Sci.* **16**, 3309-3314. doi : doi.org/10.5194/hess-16-3309-2012.

Uhlemann, S., Ulrich, C., Newcomer, M., Fiske, P., Kim, J. and Pope, J., 2022, "3D hydro geophysical characterization of managed aquifer recharges basins", *Frontiers in Earth Science*, **10**, 942737. doi : https://doi.org/10.3389/feart.2022.942737.

UNEMG, 2011. Global drylands: A UN system-wide response. United Nations Environment Management Group. Online [accessed 7 November 2016]: https://www.unep-wcmc.org/resources-and-data/global-drylands--a-un-system-wide-response.